






# Cation diffusion in polycrystalline thin films of monoclinic $\text{HfO}_2$ deposited by atomic layer deposition

Cite as: APL Mater. 8, 081104 (2020); <https://doi.org/10.1063/5.0013965>

Submitted: 15 May 2020 . Accepted: 20 July 2020 . Published Online: 04 August 2020

Michael P. Mueller , Katrin Pinggen, Alexander Hardtdegen , Stephan Aussen , Andreas Kindsmueller, Susanne Hoffmann-Eifert , and Roger A. De Souza 

[View Online](#)

Export Citation



CrossMark

## ARTICLES YOU MAY BE INTERESTED IN

## Machine learning approaches for the prediction of materials properties


APL Materials **8**, 080701 (2020); <https://doi.org/10.1063/5.0018384>

## Study of ferroelectric characteristics of $\text{Hf}_{0.5}\text{Zr}_{0.5}\text{O}_2$ thin films grown on sputtered or atomic-layer-deposited TiN bottom electrodes

Applied Physics Letters **117**, 022902 (2020); <https://doi.org/10.1063/5.0011663>

## Scattering mechanisms and mobility enhancement in epitaxial BaSnO<sub>3</sub> thin films probed via electrolyte gating

APL Materials 8, 071113 (2020); <https://doi.org/10.1063/5.0017227>



**AMERICAN  
ELEMENTS**

THE ADVANCED MATERIALS MANUFACTURER®

additive manufacturing    epitaxial crystal growth    cerium oxide polishing powder    silver nanoparticles    sputtering targets    III-IV semiconductors    CVD precursors    europium phosphors

gallium lump    glassy carbon    nanodispersions    InAs wafers    laser crystals    ultra high purity materials    MOFs

surface functionalized nanoparticle    organometallics    quantum dot    Al    Si    P    S    Cl    Ar    F    Ne

rare earth metals    photovoltaics    refractory metals    MOCVD    superconductors    transparent ceramics    ultra high purity silicon

*American Elements opens up a world of possibilities so you can **Now Invent!***

Over 15,000 certified high purity laboratory chemicals, metals, & advanced materials and a state-of-the-art Research Center. Printable GHS-compliant Safety Data Sheets. Thousands of new products. And much more. All on a secure multi-language "Mobile Responsive" platform.

desposition slugs    OLED Lighting    spintronics    solar energy

osmium    nanoribbons    thin films    chalcogenides    AuNPs

GDC    li-ion battery electrolytes    99.999% ruthenium spheres

endohedral fullerenes    copper nanoparticles    diamond micropowder

CIGS    MBE grade materials    palladium catalysts    flexible electronics

beta-barium borate    borosilicate glass    dysprosium pellets    YBCO

pyrolytic graphite    3d graphene foam    indium tin oxide    mesoporus silica

raman substrates    sapphire windows    tungsten carbide    InGaAs

barium fluoride    carbon nanotubes    lithium niobate    scandium powder

The Next Generation of Material Science Catalogs

**Now Invent.™**

perovskite crystals    yttrium iron garnet    alternative energy    h-BN

gold nanocubes    graphene oxide    macromolecules    photonics

rhodium sponge    fiber optics    beamsplitters    infrared dyes    zeolites

fused quartz    metalloceens    platinum ink    buckyballs    Ti-6Al-4V

[www.americanelements.com](http://www.americanelements.com)

# Cation diffusion in polycrystalline thin films of monoclinic $\text{HfO}_2$ deposited by atomic layer deposition

Cite as: APL Mater. 8, 081104 (2020); doi: 10.1063/5.0013965

Submitted: 15 May 2020 • Accepted: 20 July 2020 •

Published Online: 4 August 2020



Michael P. Mueller,<sup>1,a)</sup> Katrin Pinggen,<sup>1</sup> Alexander Hardtdegen,<sup>2</sup> Stephan Aussen,<sup>2</sup> Andreas Kindsmueller,<sup>3</sup> Susanne Hoffmann-Eifert,<sup>2</sup> and Roger A. De Souza<sup>1,b)</sup>

## AFFILIATIONS

<sup>1</sup>Institute of Physical Chemistry, RWTH Aachen University, 52056 Aachen, Germany

<sup>2</sup>Peter Gruenberg Institute (PGI 7 & 10), Forschungszentrum Juelich GmbH, and JARA-FIT, 52428 Juelich, Germany

<sup>3</sup>Institute of Materials in Electrical Engineering and Information Technology II, RWTH Aachen University, 52056 Aachen, Germany

<sup>a)</sup>Author to whom correspondence should be addressed: michael.patrick.mueller@rwth-aachen.de

<sup>b)</sup>Electronic mail: desouza@pc.rwth-aachen.de

## ABSTRACT

Though present in small amounts and migrating at low rates, intrinsic cation defects play a central role in governing the operational lifetime of oxide-ion conducting materials through slow degradation processes such as interdiffusion, kinetic demixing, grain growth, and creep. In this study, a new experimental approach to characterizing the behavior of such slow-moving, minority defects is presented. Diffusion is probed in samples with a constant cation-defect concentration well above the equilibrium values. This approach is applied to monoclinic hafnium dioxide,  $m\text{-HfO}_2$ . To this end, nanocrystalline thin films of  $m\text{-HfO}_2$  were prepared by atomic layer deposition. Diffusion experiments with  $\text{ZrO}_2$  as a diffusion source were performed in the temperature range  $1173 \leq T/\text{K} \leq 1323$  in air. The Zr diffusion profiles obtained subsequently by secondary ion mass spectrometry exhibited the following two features: the first feature was attributed to slow bulk diffusion and the second was attributed to combined fast grain-boundary diffusion and slow bulk diffusion. The activation enthalpy of Zr diffusion in bulk  $\text{HfO}_2$  was found to be  $(2.1 \pm 0.2)$  eV. This result is consistent with the density-functional-theory calculations of hafnium-vacancy migration in  $m\text{-HfO}_2$ , which yield values of  $\sim 2$  eV for a specific path. The activation enthalpy of the grain-boundary diffusion of  $(2.1 \pm 0.3)$  eV is equal to that for bulk diffusion. This behavior is interpreted in terms of enhanced cation diffusion along space-charge layers.

© 2020 Author(s). All article content, except where otherwise noted, is licensed under a Creative Commons Attribution (CC BY) license (<http://creativecommons.org/licenses/by/4.0/>). <https://doi.org/10.1063/5.0013965>

## I. INTRODUCTION

Crystalline ion conductors generally consist of a sublattice of mobile ions and one or more sublattices of immobile ions. The latter form a stable framework through which the mobile ions can migrate. In reality, however, no ion is completely immobile in a crystalline solid: the “immobile” ions are merely considerably less mobile than the “mobile” ions. In addition, this has to be the case if the stable phase is a solid and not a liquid. The issue, therefore, is actually one of the relative diffusion rates.

Taking the case of  $\text{AO}_2$  oxides that adopt the fluorite and related structures, oxides such as  $\text{ZrO}_2$ ,  $\text{HfO}_2$ ,  $\text{CeO}_2$ ,  $\text{ThO}_2$ ,  $\text{UO}_2$ , and  $\text{PuO}_2$ , one recognizes that they all have mobile oxide ions and relatively immobile cations.<sup>1–4</sup> Indeed, solid solutions based on  $\text{ZrO}_2$  or  $\text{CeO}_2$  are utilized as oxide-ion conducting electrolytes.<sup>5–8</sup> Oxide-ion transport in  $\text{HfO}_2$ , ignored for many years, is now attracting attention because the phenomenon can be put to use in resistive switching memory devices.<sup>9–15</sup> In addition, oxygen diffusion plays a central role in the compatibility of nuclear fuel rods with metal claddings and in the behavior of certain fission products.<sup>16–19</sup>

Studying the diffusion of a crystal's "immobile" ions experimentally is difficult because the number of defects responsible for diffusion is generally low and the activation enthalpy of defect migration is generally high, which means that diffusion coefficients are necessarily very small. High temperatures and long diffusion times are thus needed to achieve measurable diffusion lengths, conditions that are often accompanied by complicating effects (e.g., diffusion specimens showing morphological changes). If one manages to obtain diffusion data of sufficient quality, one faces the further problem of interpreting the measured activation enthalpy of diffusion,  $\Delta H_D$ . Even in the simplest case,  $\Delta H_D$  is the sum of two individual enthalpies,  $\Delta H_{\text{mig}}$ , the activation enthalpy of defect migration, and  $\Delta H_{\text{gen}}$ , the enthalpy of defect generation,

$$\Delta H_D = \Delta H_{\text{mig}} + \Delta H_{\text{gen}}. \quad (1)$$

$\Delta H_{\text{gen}}$  describes how the concentration of the defect responsible for diffusion,  $c_{\text{def}}$ , changes with temperature  $T$ ,

$$\Delta H_{\text{gen}} = -k_B [d \ln c_{\text{def}}/d(1/T)]. \quad (2)$$

For minority defects, neither  $\Delta H_{\text{mig}}$  nor  $\Delta H_{\text{gen}}$  is independently accessible from experiment.

Simulation techniques, based either on Density-Functional-Theory (DFT) calculations or on calculations with Empirical Pair Potentials (EPP), can prove helpful by providing both  $\Delta H_{\text{mig}}$  and the relevant defect energies entering  $\Delta H_{\text{gen}}$ . Help is not always guaranteed, however. In the case of cation diffusion in Gd-doped  $\text{CeO}_2$ , for example, the experimental value of  $\Delta H_D \approx 5.5$  eV is substantially lower than the sum of the (DFT) computational values for vacancy migration, with  $\Delta H_{\text{mig,v}} = 4.4$  eV and  $\Delta H_{\text{gen,v}} = 6.9$  eV.<sup>3,20,21</sup> Similarly for  $\text{UO}_2$ , the experimental value of  $\Delta H_D \approx 5.6$  eV is substantially lower than the (EPP) computational values of  $\Delta H_{\text{mig,v}} = 6$  eV and  $\Delta H_{\text{gen,v}} = 6.5$  eV.<sup>19</sup> Values for cation interstitials show even larger discrepancies.

The interpretation of the experimental values of  $\Delta H_D$  would be simplified if the concentration of the defects responsible for diffusion could be fixed over an appropriate range of temperatures so that  $\Delta H_{\text{gen}}$  goes to zero. For majority defects, a suitable dopant and suitable thermodynamic conditions may serve to fix  $c_{\text{def}}$  (e.g., in Gd-doped  $\text{CeO}_2$  under oxidizing conditions, the concentration of oxygen vacancies is fixed by the gadolinium dopant concentration). For minority defects, however, a variety of intrinsic and extrinsic defect reactions determines  $c_{\text{def}}$ . That is, the concentrations of minority defects are dictated by thermodynamics. In general,  $c_{\text{def}}$  will, therefore, vary with temperature, giving rise to non-zero  $\Delta H_{\text{gen}}$ . For the case of Gd-doped  $\text{CeO}_2$  mentioned above, with gadolinium fixing the oxygen vacancy concentration,  $\Delta H_{\text{gen}}$  for cation vacancies is equal to  $\Delta H_{\text{Sch}}$  (the enthalpy of the Schottky disorder). One way to avoid this problem, then, is to study samples that are not in equilibrium so that thermodynamics is removed from the problem. We propose to achieve this by investigating cation diffusion in metastable samples in which the concentration of the minority defects is fixed through kinetics, i.e., through the preparation procedure.

In this study, such samples are fabricated by Atomic Layer Deposition (ALD), the established industrial process for growing nanometer-thin, homogeneous insulating  $\text{HfO}_2$  thin films for use in high-permittivity metal gate transistors, flash memory, and also

a new type of Random Access Memory (RAM), the one utilizing redox-based Resistive switching (ReRAM).<sup>22–25</sup> The primary advantage for this study is that this method offers the possibility of producing polycrystalline films of monoclinic  $\text{HfO}_2$  ( $m\text{-HfO}_2$ ) at low temperatures.<sup>26</sup> The low temperatures provide the sluggish kinetics required so that equilibrium is not achieved for the cation sublattice. An additional advantage is that ALD produces films that are free of Si (whose presence complicates the study of diffusion in  $\text{Al}_2\text{O}_3$  oxides<sup>27–30</sup>). The use of  $\text{HfO}_2$  also offers the advantage of using Zr as a chemically similar species to study cation diffusion rather than using expensive (and hard to process) Hf isotopes.

## II. METHODOLOGY

### A. Experimental

As noted above, previous studies have shown that silica impurities severely impact the oxygen diffusion behavior in  $m\text{-HfO}_2$ .<sup>27–30</sup> For this reason, the industrial standard, silicon wafers are omitted for this study. While ALD makes use of Si-free precursors and, thus, yields Si-free samples, the film substrates remain as a possible source of Si, particularly due to silica residues remaining on the surface after polishing. For this reason, the amount of Si impurities was examined on different substrates [ $\text{DyScO}_3$ ,  $(\text{LaAlO}_3)_{0.3}(\text{Sr}_2\text{TaAlO}_6)_{0.7}$ ,  $\text{NdGaO}_3$ ,  $\text{SrTiO}_3$ ,  $\text{Al}_2\text{O}_3$ , and YSZ] with Secondary Ion Mass Spectrometry (SIMS).  $\text{DyScO}_3$  delivered the best results, with the least amount of Si at the interface of the film and substrate. We attribute this behavior to the self-cleaning effect of perovskite-type systems.<sup>31–33</sup> Reactive ion beam etching on the substrate surface followed by  $\text{HfO}_2$  deposition showed no discernible influence on the amount of Si. Thus, polished  $\text{DyScO}_3$  single crystals were used as substrates for the  $\text{HfO}_2$  thin films.

For the plasma assisted ALD process, tetrakis(ethylmethylamino) hafnium ( $\text{TEMAH}$ ,  $\geq 99.99\%$  trace metal basis excluding  $\sim 2000$  ppm Zr, SAFC Hitech®) was used as a precursor to deposit  $\text{HfO}_2$  at  $T = 573$  K as a thin, amorphous layer with embedded  $m\text{-HfO}_2$  nanocrystals of about 3 nm in diameter.<sup>26</sup> An oxygen plasma was used as a co-reactant. The ALD process was performed in a Flexal™ ALD tool (Oxford Instruments Plasma Technologies, Bristol, United Kingdom). Then, a thin layer of  $\text{ZrO}_2$  was employed as a diffusion source, deposited by RF-magnetron sputtering (an output power of 60 W) from a Zr-target at room temperature under 0.01 mbar pressure in a mixture of 38 sccm Ar and 2 sccm  $\text{O}_2$ . These conditions resulted in a deposition rate of 0.82 nm/min. Our aim was to deposit 40 nm of  $\text{ZrO}_2$  on 100 nm of  $\text{HfO}_2$ .

Diffusion anneals were carried out in a  $\text{MoSi}_2$  furnace in air inside a closed  $\text{Al}_2\text{O}_3$  vessel. The heating rate was 500 K/h for all temperatures. Samples were quenched after the anneal by removing them from the  $\text{MoSi}_2$  furnace and transferring them to another furnace with a temperature of 873 K. They were then cooled to room temperature with a cooling rate of 500 K/h. This procedure was employed to avoid cracking of the samples through very rapid cooling.

Grazing incidence x-ray diffractograms obtained with a X'Pert MRD system (PANalytical, Almelo, The Netherlands) indicated the existence of a single monoclinic phase after annealing the sample in air at 1273 K for 20 h. After 20 h at 1373 K, both monoclinic and cubic phases were found. After 10 h at 1423 K, only the cubic phase

was found. We assume that the phase transition occurs as a result of  $\text{Dy}^{3+}$  and  $\text{Sc}^{3+}$  diffusing in from the substrate (detected by ToF-SIMS analysis; see below), similar to the stabilization of the cubic phase of  $\text{ZrO}_2$  upon  $\text{Y}^{3+}$  doping.<sup>34</sup> To ensure that cation diffusion data refer to the monoclinic phase of  $\text{HfO}_2$ , only samples annealed at temperatures below 1373 K were subjected to analysis.

Scanning electron microscopy (SEM) images of the thin-film samples after the analysis were taken with an SU8000 system (Hitachi, Tokyo, Japan). From these images, we determined that the grain size varied between 20 nm and 90 nm, depending on the annealing temperature. Interference microscopy (NT1100, Veeco Instruments, Inc., NY, USA) indicated a roughness of  $\pm 2$  nm for the areas relevant to ToF-SIMS analysis ( $100 \times 100 \mu\text{m}^2$ ).

ToF-SIMS depth profiles were obtained<sup>35,36</sup> on a ToF-SIMS IV machine equipped with a ToF-SIMS V analyzer (ION-TOF GmbH, Münster, Germany). 25 keV  $\text{Ga}^+$  ions, rastered over an area of  $100 \times 100 \mu\text{m}^2$ , were used to generate secondary ions. Measurements were performed with a ToF cycle time of 60  $\mu\text{s}$  in the bunched mode,<sup>35</sup> and negative secondary ions were detected. Preliminary studies indicated that the secondary-ion intensities of  $\text{MeO}^-$  species ( $\text{Me} = \text{Hf/Zr}$ ) under  $\text{Cs}^+$  bombardment were higher than those of  $\text{Me}^+$  species under  $\text{O}_2^+$  bombardment. Therefore, 2 keV  $\text{Cs}^+$  ions were used for sputter etching the sample surface, typically over an area of  $400 \times 400 \mu\text{m}^2$ . Charge compensation was accomplished with a beam of low-energy ( $<20$  eV) electrons. Secondary-ion intensities of  $\text{MeO}^-$  species were normalized to the intensity of  $^{18}\text{O}^-$  and to the maximum intensity of the profiles. Crater depths were determined post-analysis by interference microscopy.

## B. Computational

All DFT calculations were performed within the generalized gradient approximation after Perdew, Burke, and Ernzerhof (PBE).<sup>37</sup> The potentials generated by the projector augmented wave<sup>38</sup> method were used with an energy cutoff of 500 eV. Calculations were performed for a periodic  $2 \times 2 \times 2$  supercell of  $m\text{-HfO}_2$  containing 31 Hf atoms and 64 O atoms (since a  $\text{Hf}^{4+}$  species was removed, the behavior of a charged vacancy is considered). k-points were generated by a  $2 \times 2 \times 2$  Monkhorst-Pack mesh.<sup>39</sup> For convergence criteria, electronic convergence was set to  $1 \times 10^{-4}$  and ionic convergence was set to  $1 \times 10^{-3}$ . The Climbing-Image Nudged Elastic Band (CI-NEB)<sup>40–42</sup> method was used to determine the energy of the transition state over three images along the cation jump. The Vienna *ab initio* simulation package was used.<sup>43,44</sup>

## III. RESULTS

### A. Experimental

The sample geometry and the investigated length-scale of the diffusion samples are indicated in Fig. 1(a). Figure 1(b) shows the intensity profiles for  $\text{ZrO}^-$  and  $\text{HfO}^-$  secondary ions across the structure obtained prior to the diffusion anneal by SIMS depth profiling. The two different layers are well-defined and homogeneous. Examining the interface region, we find that the range of depths over which the  $\text{ZrO}^-$  signal decreases is approximately equal to the range of depths over which the  $\text{HfO}^-$  signal increases. This

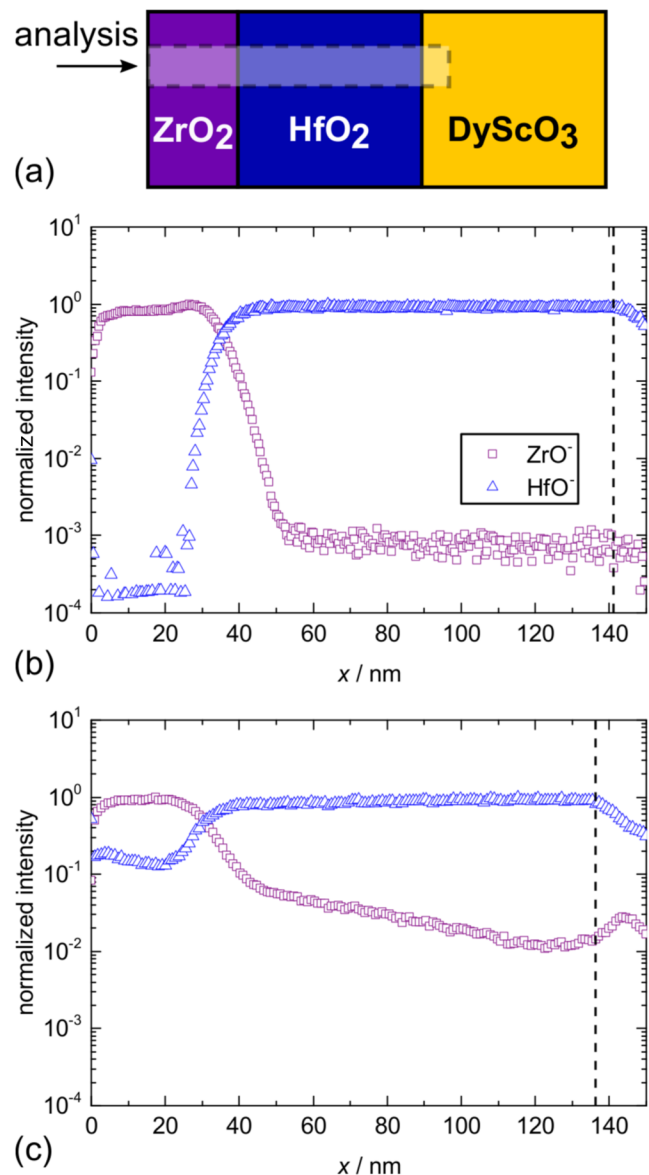


**FIG. 1.** (a) Sketch of the sample geometry and the analyzed region; (b) normalized intensities of  $\text{ZrO}^-$  and  $\text{HfO}^-$  secondary ions obtained by ToF-SIMS depth profiling for a sample prior to the diffusion anneal; the vertical dashed line indicates the interface with the  $\text{DyScO}_3$  substrate; and (c) normalized intensities of  $\text{ZrO}^-$  and  $\text{HfO}^-$  secondary ions obtained by ToF-SIMS depth profiling for a sample annealed at  $T = 1273$  K for  $t = 20$  h.

suggests that the broadening of the signals comes from the samples, i.e., it is due to the roughness of the  $\text{ZrO}_2$  surface and/or the  $\text{ZrO}_2/\text{HfO}_2$  interface. If direct recoil and ion beam mixing (SIMS effects) were responsible, the two ranges of depths would not be similar. At a depth of  $\sim 140$  nm, the hafnia layer ends and the substrate layer begins, which is the expected result according to the process specifications.

After diffusion annealing, the intensity profile of  $\text{ZrO}^-$ , as shown in Fig. 1(c), still displays a constant plateau in the  $\text{ZrO}_2$  layer; at the  $\text{ZrO}_2|\text{HfO}_2$  interface, the broadening is less steep than in the sample prior to the diffusion anneal, suggesting cation diffusion; and a long profile, extending from  $\approx 45$  nm up to the substrate at  $\sim 135$  nm, has developed. The position of the  $\text{HfO}_2|\text{DyScO}_3$  interface has apparently shifted slightly, but careful examination revealed that it is actually a shift of the  $\text{ZrO}_2|\text{HfO}_2$  interface. The thickness of the  $\text{HfO}_2$  layer has not changed. We ascribe this shift to the densification of the  $\text{ZrO}_2$  layer upon thermal treatment (since it was sputtered at room temperature) and a consequent reduction in film thickness. Near the substrate, an upturn in the  $\text{ZrO}^-$  intensity profile is observed. We attribute this upturn to a SIMS artifact that arises as the sputter front passes through the interface from the  $\text{HfO}_2$  film to the  $\text{DyScO}_3$  substrate. Simulations of diffusion (see below) did not reproduce this upturn. The obvious interpretation of the profile is that the broadening is due to diffusion in bulk  $m\text{-HfO}_2$  and the long profile is due to a combination of fast grain-boundary diffusion and slow diffusion out of the boundary. Given that the area of the ToF-SIMS analysis was  $100\ \mu\text{m}^2$  and the area of a single grain is of the order of  $10^3\ \text{nm}^2$ , the profile refers to the average over  $\sim 10^5$  grains and their grain boundaries. The diffusion profile obtained for  $\text{HfO}^-$  shows similar, though not identical, behavior. Going from the substrate toward the surface, one sees a constant plateau of  $\text{HfO}^-$  in the  $\text{HfO}_2$  layer, a decrease corresponding to diffusion and to the broadening arising from interfacial roughness, but then, an increase in  $\text{HfO}^-$  intensity toward the surface. This suggests surface diffusion of Hf from the film to the external  $\text{ZrO}_2$  surface and diffusion inward from this surface. In the following, we do not consider the  $\text{HfO}^-$  profiles further, but focus on the  $\text{ZrO}^-$  profiles in  $\text{HfO}_2$ .

Given the complexity of the diffusion problem—diffusion along two different paths (bulk and grain boundary) in a medium of finite extent from a non-trivial initial distribution—we chose to solve the diffusion equation numerically in two dimensions in order to obtain the relevant diffusion coefficients. To this end, Finite-Element-Method (FEM) simulations were implemented in COMSOL Multiphysics® (COMSOL AB, Stockholm, Sweden) for a simulation box of length  $l_{\text{film}}$  and of width  $d_{\text{gr}} + d_{\text{gb}}$  (of which  $d_{\text{gb}}$  is the region within which fast grain-boundary diffusion takes place). Bulk and grain-boundary diffusion coefficients were assumed to be isotropic and the same for both  $\text{ZrO}_2$  and  $\text{HfO}_2$  layers. The assumption of isotropic diffusion coefficients for non-isotropic  $m\text{-HfO}_2$  is reasonable since each diffusion profile is an average over  $\sim 10^5$  grains (and the grains show no preferred orientation according to XRD scans). In the simulations,  $l_{\text{film}}$  was set to the film's thickness,  $d_{\text{gb}}$  was chosen to be 1 nm, and  $d_{\text{gr}}$  was assumed to be constant at each temperature (i.e., grain growth was assumed to take place faster than in diffusion), with values taken from the SEM images. The intensity profile prior to the diffusion anneal [e.g., Fig. 1(b)] was used as the initial condition.

Figure 2(a) shows a 2D concentration heat map obtained from an FEM simulation of zirconium diffusion in the layer structure. The different regions and grain boundaries of the model are clearly visible in the heat map. The concentration heat map was averaged parallel to the surface to obtain a simulated diffusion profile that was compared visually with the experimental data.  $D_{\text{b}}$ ,  $D_{\text{gb}}$ , and  $d_{\text{gr}}$  were varied until good agreement was found, as shown in Fig. 2(b).

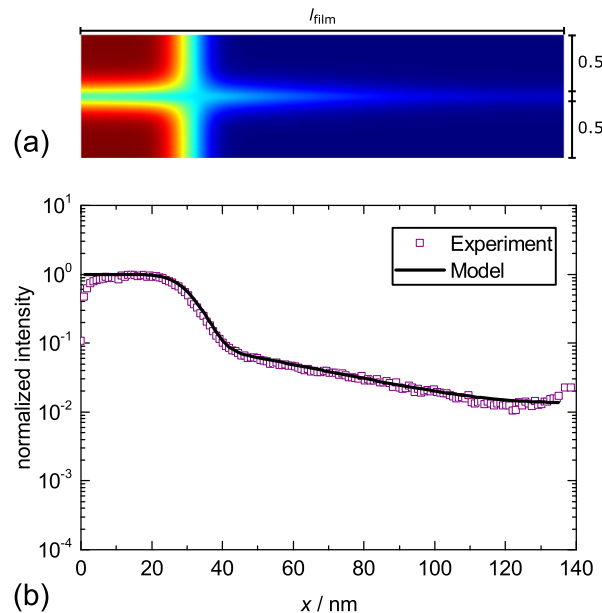


**FIG. 2.** Continuum simulations of zirconium diffusion into a polycrystalline thin-film at  $T = 1273$  K for  $t = 20$  h. (a) 2D concentration heat map (dark red: high concentration; dark blue: low concentration) of the simulation cell, with the grain boundary running through the center of the cell; (b) comparison of simulated and experimental diffusion profiles.

(Note that only small adjustments to  $d_{\text{gr}}$  from the SEM values were necessary.) Unlike the standard analysis of grain-boundary diffusion,<sup>45,46</sup> which yields the grain-boundary diffusion product  $d_{\text{gb}}D_{\text{gb}}$ , these simulations give the grain-boundary diffusion coefficient  $D_{\text{gb}}$  since  $d_{\text{gb}}$  is explicitly specified. This means that the values of  $D_{\text{gb}}$  are specific to the value of  $d_{\text{gb}}$ ; if accelerated diffusion takes place within a region wider or narrower than  $d_{\text{gb}} = 1$  nm, then the values we obtained for  $D_{\text{gb}}$  will change (see later). Diffusion coefficients of zirconium obtained for the  $m\text{-HfO}_2$  films as a function of annealing temperature are plotted in Fig. 3.  $D_{\text{gb}}$  is seen to be  $\sim 3$  orders of magnitude higher than  $D_{\text{b}}$  at all temperatures. For bulk diffusion of zirconium in  $m\text{-HfO}_2$ , an activation enthalpy of  $\Delta H_{\text{b}} = (2.1 \pm 0.2)$  eV is obtained. The activation enthalpy of zirconium diffusion in the grain boundary is the same at  $\Delta H_{\text{gb}} = (2.1 \pm 0.3)$  eV.

## B. Computational

Cations in the cubic  $\text{AO}_2$  fluorite structure ( $c\text{-AO}_2$ ) sit on a single crystallographic site and have 8 oxygen ions as the nearest neighbors and 12 cations as the next-nearest neighbors. (Oxide ions are fourfold coordinated by A cations and are also located on a single crystallographic site.) For cation migration by a vacancy mechanism, cations jump along the  $\langle 110 \rangle$  directions to vacant sites.<sup>3,47–49</sup> The high degree of symmetry in  $c\text{-AO}_2$  leads to all 12 possible jumps being symmetry equivalent. This is not the case in  $m\text{-HfO}_2$ , however, where (because of the monoclinic distortion) hafnium is sevenfold coordinated by oxygen and two different oxygen sites exist, half of which are threefold and half are fourfold coordinated. Although the number of next-nearest neighboring hafnium ions and, thus, the



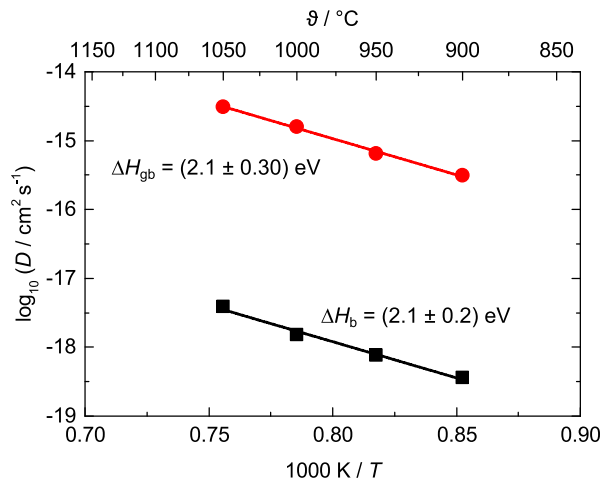


**FIG. 3.** Diffusion coefficients of zirconium in bulk  $m$ -HfO<sub>2</sub> and along its grain boundaries as a function of inverse temperature.

number of possible jumps remain to be twelve (i.e., the same as in  $c$ -AO<sub>2</sub>), many of these jumps are no longer symmetry equivalent. In fact, only four of these jumps are symmetry equivalent, leaving eight distinct possible jumps [see Fig. 4(a)], in contrast to the single, unique jump of the cubic structure. We used CI-NEB calculations to calculate the migration barriers by a vacancy mechanism for these hafnium ion jumps in the monoclinic structure. The results are plotted in Fig. 4(b).

The activation barriers are seen to vary from 1.8 eV to 4.8 eV. This range of values does not seem to be consistent with those from

the experiments. One critical point, however, is the combinations of jumps that are required so that hafnium can migrate through the cell from one side to the other. In this regard, jumps 3 and 8, with 2.1 eV and 1.8 eV, together provide a path through the cell in the  $\langle 001 \rangle$  direction. The second critical point concerns the jump rates at the temperatures of the experiments,  $\Gamma_v = v_0 e^{\Delta S_{\text{mig},v}/k_B} e^{-\Delta H_{\text{mig},v}/k_B T}$ . Assuming that the attempt frequencies ( $v_0$ ) and the activation entropies of migration ( $\Delta S_{\text{mig},v}$ ) do not vary much for the various jumps, one finds that, at  $T = 1100$  K, jumps over the other barriers occur far less frequently in comparison (for 3 eV, a factor of  $10^4$  less; for 4.8 eV, a factor of  $10^{12}$  less). Hence, hafnium migration in other directions will not be observed at the temperatures of the experiments because those paths have substantially higher barriers. We thus conclude that the activation energy of hafnium-vacancy migration at the temperatures of interest in a polycrystal with randomly oriented grains will be given by the (largest) migration barrier in the  $\langle 001 \rangle$  direction,  $\sim 2$  eV.

## IV. DISCUSSION

### A. Bulk diffusion

The good agreement between  $\Delta H_D$  obtained experimentally and  $\Delta H_{\text{mig},v}$  obtained computationally for cation transport in  $m$ -HfO<sub>2</sub> strongly suggests [see Eq. (1)] that  $\Delta H_{\text{gen},v}$  for our non-equilibrium samples was zero and, hence, that the concentration of hafnium vacancies does not vary with temperature, in accord with our initial premise. The investigation of non-equilibrium samples thus opens a new avenue to studying the migration of slow-moving minority defects.

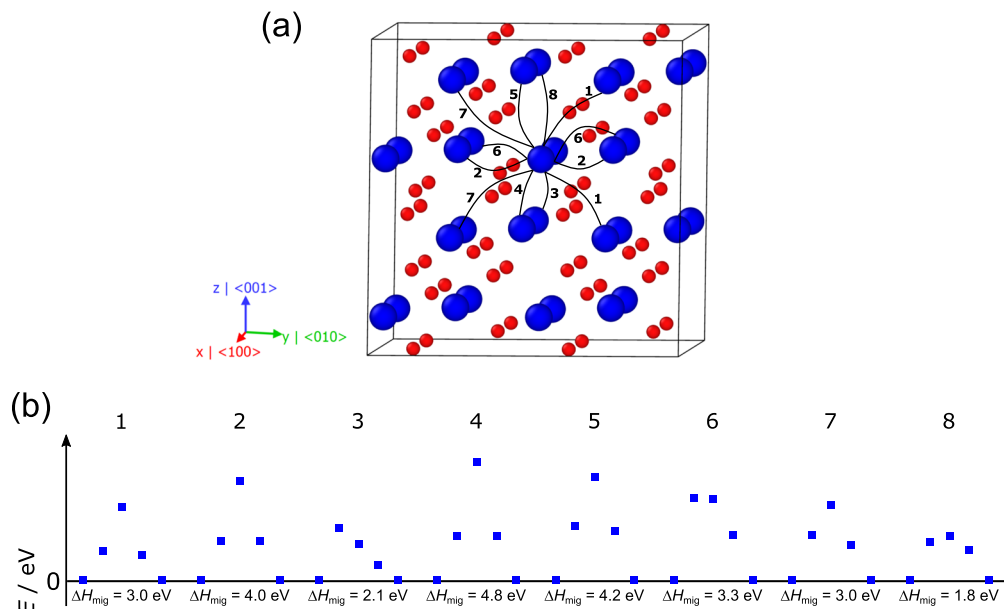


**FIG. 4.** (a) Structure of  $m$ -HfO<sub>2</sub>, indicating the eight symmetry-inequivalent jumps of a hafnium cation by a vacancy mechanism. Hafnium ions are shown in blue, and oxygen ions are shown in red. Lines do not indicate exact jump paths. This figure is created with OVITO.<sup>50</sup> (b) Schematic energy landscapes of the different jumps in  $m$ -HfO<sub>2</sub> showing the migration barriers. Each jump consists of three images and start/end positions. The images are not equidistant.

Compared with the values obtained computationally for cation-vacancy migration in other AO<sub>2</sub> systems— $\Delta H_{\text{mig},v}$  is over 4 eV for CeO<sub>2</sub><sup>3</sup> and over 5 eV for UO<sub>2</sub><sup>48,49,51</sup> and ZrO<sub>2</sub><sup>52</sup>—we find that  $\Delta H_{\text{mig},v}$  for cations in *m*-HfO<sub>2</sub> has similar values (3 eV–5 eV) but also two substantially lower values ( $\approx 2$  eV). The difference between these three oxides and HfO<sub>2</sub> is the crystal symmetry: CeO<sub>2</sub> and UO<sub>2</sub> adopt the high-symmetry cubic form (and ZrO<sub>2</sub> was considered in the computer simulations<sup>52</sup> as a hypothetical cubic structure), whereas HfO<sub>2</sub> has a strongly distorted monoclinic structure.

Metlenko *et al.*<sup>53</sup> proposed a general rule for the effect of structural perturbations on ion migration. They hypothesized that, for ions that are highly mobile in a given structure, structural perturbations lead to a decrease in ion mobility, whereas for ions that are immobile, structural perturbations lead to an increase. Indeed, isothermal rates of oxide-ion transport in monoclinic and tetragonal ZrO<sub>2</sub> and HfO<sub>2</sub> are found to be much lower than in the cubic form.<sup>54–57</sup> We would expect, therefore, the strong structural perturbation of *m*-HfO<sub>2</sub> to lead to higher rates of cation diffusion than in the cubic counterparts. In the present case, one could argue more specifically in terms of the oxygen coordination of the cations. A sevenfold coordination of hafnium by oxygen increases their mobility compared to that in an eightfold coordination; for CeO<sub>2</sub> and UO<sub>2</sub>, such an enhancement of cation mobility is found in the presence of oxygen vacancies<sup>58,59</sup> (specifically, an increase in grain-boundary mobility was observed in an oxygen-poor atmosphere). If we understand oxygen vacancies in a cubic fluorite lattice as a perturbation of the eightfold coordination of the A cation toward a sevenfold coordination, then the sevenfold coordination of hafnium in the monoclinic crystal structure might increase the cation mobility and explain the low migration enthalpies.

Another benefit of our approach is that it allows us to estimate  $n_v$ , the site fraction of cation vacancies in our samples. Since we can express the bulk diffusion coefficients in terms of  $n_v$ , a jump distance  $d_v$ , and the jump rate  $\Gamma_v$ ,

$$D_b = n_v d_v^2 \Gamma_v, \quad (3)$$

we find, with  $d_v = 0.36$  nm,  $v_0 = 10^{13}$  s<sup>−1</sup>, and  $\Delta S_{\text{mig},v}/k_B = 0$ ,  $n_v \sim 10^{-8}$ . This is consistent with cation vacancies being the minority defects in acceptor-doped AO<sub>2</sub> systems.

In Fig. 5, we compare our bulk cation diffusion coefficients with selected experimental data reported in the literature. If one considers the datasets B, C, and D together and extrapolates the data to the lower temperatures of our experiments, one finds that our cation bulk diffusivities are significantly higher than the ones found in similar fluorite-structured systems and the activation enthalpy is significantly lower. Beschnitt and De Souza<sup>20</sup> reported that  $\Delta H_b = (5.5 \pm 0.4)$  eV for Zr diffusion in Gd-doped (0.5%) CeO<sub>2</sub> (cubic); Tesch *et al.*<sup>60</sup> reported that  $\Delta H_b = (8.0 \pm 0.3)$  eV for Hf diffusion in Er<sub>2</sub>O<sub>3</sub>-stabilized (10%) HfO<sub>2</sub> (cubic); and Swaroop *et al.*<sup>61</sup> reported that  $\Delta H_b = (5.3 \pm 0.9)$  eV for Hf diffusion in 3 mol. % Y<sub>2</sub>O<sub>3</sub>-stabilized ZrO<sub>2</sub> (tetragonal). We attribute the difference to our samples having a higher site fraction of cation vacancies and a lower activation barrier of migration (being monoclinic rather than cubic or tetragonal).

## B. Grain-boundary diffusion

Fast grain-boundary diffusion of cations has also been previously observed in cubic AO<sub>2</sub>-type oxides.<sup>20,61</sup> In some cases, e.g.,

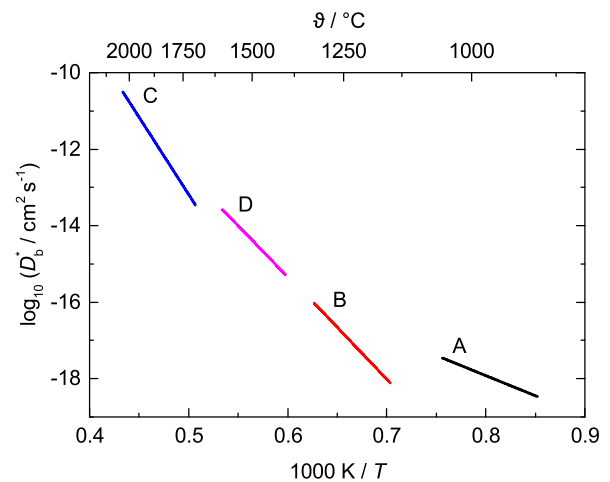


**FIG. 5.** Comparison of diffusion coefficients for cation bulk diffusion in selected fluorite-based oxides: (A) Zr in *m*-HfO<sub>2</sub>, this study; (B) Zr in Gd-doped (0.5%) CeO<sub>2</sub>,<sup>20</sup> (C) Hf in Er<sub>2</sub>O<sub>3</sub>-stabilized (10%) HfO<sub>2</sub>,<sup>60</sup> and (D) Hf in 3 mol. % Y<sub>2</sub>O<sub>3</sub>-stabilized ZrO<sub>2</sub>.<sup>61</sup>

Ref. 20, the ratio of the activation enthalpies was also found to be  $r = \Delta H_{\text{gb}}/\Delta H_b \approx 1$ , rather than the expected<sup>45,46,62–64</sup>  $r \approx 0.5$ . This would suggest that the traditional picture of fast grain-boundary diffusion taking place along the grain-boundary core does not hold here (as it requires  $r \approx 0.5$ ). The alternative possibility is fast diffusion along space-charge layers. In addition, the presence of such layers at grain boundaries is well established for various acceptor-doped AO<sub>2</sub>-type oxides<sup>65–70</sup> in which positive grain-boundaries are compensated by negative space-charge layers in which (positive) oxygen vacancies are depleted and (negative) acceptor dopants are accumulated. The important point in this case is that cation vacancies, as negatively charged defects, are also accumulated in the space-charge layers. It is this accumulation that gives rise to the enhanced rates of cation diffusion.<sup>71</sup> In the following, we show that this picture is consistent with the experimental data and we extract the space-charge potential. The comparison is made on the basis of the grain-boundary diffusion product,  $D_{\text{gb}}d_{\text{gb}}$ , for three reasons. First, it is the quantity that is usually extracted from diffusion experiments in Harrison-type B kinetics. Second, it avoids the arbitrary specification of  $d_{\text{gb}}$  used Sec. III A. Third, it is the quantity that comes out of the space-charge analysis.<sup>71</sup>

Incidentally, one can easily discount the alternative explanation that the observed behavior is simply due to more cation vacancies being present in the grain-boundary core. This ignores that space-charge layers are present at grain boundaries in acceptor-doped AO<sub>2</sub> systems. In addition, it requires the migration barrier for cation vacancies at the boundary to be the same as in the bulk: this is extremely unlikely. In addition, it requires the cation vacancies to be neutral (if they were charged, the question of space-charge zones raises its head).

Measurements of leakage currents and subsequent analysis in line with the discussion of Gritsenko *et al.*<sup>72</sup> give a range for the concentration of acceptor concentrations  $c_{\text{acc}}$  in the HfO<sub>2</sub> thin films, which amounts to  $10^{19}$  cm<sup>−3</sup>– $10^{20}$  cm<sup>−3</sup>. Using a range of  $\epsilon_r = 15$ –25

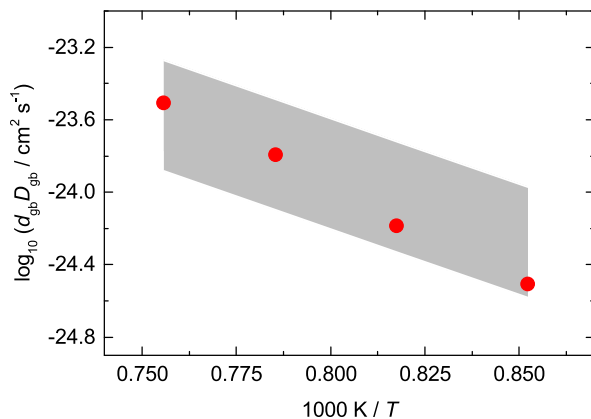


**FIG. 6.** Comparison of  $D_{gb}d_{gb}$  values obtained experimentally (red circles) and predicted from a space-charge potential of  $\Phi_0 \approx 0.82$  V (gray area). The predicted range of  $D_{gb}d_{gb}$  is obtained for  $10^{19} \leq c_{acc}/\text{cm}^{-3} \leq 10^{20}$  and  $15 \leq \epsilon_r \leq 25$ .

for the relative dielectric permittivity of  $m\text{-HfO}_2$ ,<sup>22,73–75</sup> we found that a space-charge potential  $\Phi_0 \approx 0.82$  V is consistent with the experimental data (see Fig. 6). The impact of the range in acceptor concentration and dielectric permittance is rather small, and the space-charge potential is neither unreasonably high nor low.<sup>65,76</sup>

## V. CONCLUSION

Studying experimentally the diffusion of “immobile” minority species, widely considered as very challenging, is achieved by utilizing a low-temperature preparation method, ALD, to prepare non-equilibrium samples in which the concentration of the minority defects is constant. The behavior of these defects was probed subsequently by performing cation diffusion experiments. The measured diffusion profiles display two features, are analyzed by solving the diffusion equation numerically, and yield bulk diffusion coefficients and grain-boundary diffusion coefficients.

The activation enthalpy of bulk diffusion is  $\Delta H_b = (2.1 \pm 0.2)$  eV and significantly lower compared to other oxide systems of comparable structures. DFT calculations for the individual cation jumps in  $m\text{-HfO}_2$  give mostly migration enthalpies of 3 eV–5 eV, which agree with the values obtained for the other  $\text{AO}_2$  systems. However, two jumps have significantly lower values ( $\approx 2$  eV) and allow long-range diffusion through the bulk. We argue that the other jumps occur far less frequently and the DFT results, thus, agree with our experiments. The difference in the activation enthalpy of bulk diffusion between other  $\text{AO}_2$  systems and  $m\text{-HfO}_2$  is attributed to the structural perturbations in the monoclinic system, which are hypothesized to increase the ion mobility for immobile ions (such as cations in oxide-ion conducting  $\text{AO}_2$  systems).

The observed grain-boundary diffusion activation enthalpy is the same as the activation enthalpy for bulk diffusion with  $\Delta H_{gb} = (2.1 \pm 0.3)$  eV. This contradicts the traditional picture of fast grain-boundary diffusion along the grain-boundary core, and we, instead, suggest fast cation diffusion along space-charge layers. This theory is supported by the prediction of a reasonable space-charge potential for our investigated system.

## SUPPLEMENTARY MATERIAL

See the [supplementary material](#) for the x-ray diffractograms of the  $\text{HfO}_2$  films and SEM images of the annealed samples.

## ACKNOWLEDGMENTS

The authors acknowledge funding from the German Research Foundation (DFG) within the collaborative research center, Grant No. SFB 917, “Nanoswitches.” We would like to thank Hehe Zhang for the SEM images. Simulations were performed with computing resources granted by RWTH Aachen University under Project No. rwth0310.

## DATA AVAILABILITY

The data that support the findings of this study are available from the corresponding author upon reasonable request.

## REFERENCES

- K. Ando and Y. Oishi, *J. Nucl. Sci. Technol.* **20**, 973 (1983).
- C. Sari, *J. Nucl. Mater.* **78**, 425 (1978).
- S. Beschmitt, T. Zacherle, and R. A. De Souza, *J. Phys. Chem. C* **119**, 27307 (2015).
- B. W. Busch, W. H. Schulte, E. Garfunkel, T. Gustafsson, W. Qi, R. Nieh, and J. Lee, *Phys. Rev. B* **62**, R13290 (2000).
- H. Inaba and H. Tagawa, *Solid State Ionics* **83**, 1 (1996).
- J. C. Boivin and G. Mairesse, *Chem. Mater.* **10**, 2870 (1998).
- J. A. Kilner, *Solid State Ionics* **129**, 13 (2000).
- A. Orera and P. R. Slater, *Chem. Mater.* **22**, 675 (2010).
- V. Milo, C. Zambelli, P. Olivo, E. Pérez, M. K. Mahadevaiah, O. G. Ossorio, C. Wenger, and D. Ielmini, *APL Mater.* **7**, 081120 (2019).
- F. Cüppers, S. Menzel, C. Bengel, A. Hardtdegen, M. von Witzleben, U. Böttger, R. Waser, and S. Hoffmann-Eifert, *APL Mater.* **7**, 091105 (2019).
- G. H. Kim, H. Ju, M. K. Yang, D. K. Lee, J. W. Choi, J. H. Jang, S. G. Lee, I. S. Cha, B. K. Park, J. H. Han, T.-M. Chung, K. M. Kim, C. S. Hwang, and Y. K. Lee, *Small* **13**, 1701781 (2017).
- S. Clima, Y. Y. Chen, C. Y. Chen, L. Goux, B. Govoreanu, R. Degraeve, A. Fantini, M. Jurczak, and G. Pourtois, *J. Appl. Phys.* **119**, 225107 (2016).
- P. Calka, M. Sowinska, T. Bertaud, D. Walczyk, J. Dabrowski, P. Zaumseil, C. Walczyk, A. Gloskovskii, X. Cartoixa, J. Suñé, and T. Schroeder, *ACS Appl. Mater. Interfaces* **6**, 5056 (2014).
- M. Lanza, K. Zhang, M. Porti, M. Nafria, Z. Y. Shen, L. F. Liu, J. F. Kang, D. Gilmer, and G. Bersuker, *Appl. Phys. Lett.* **100**, 123508 (2012).
- B. Govoreanu, G. S. Kar, Y.-Y. Chen, V. Paraschiv, S. Kubicek, A. Fantini, I. P. Radu, L. Goux, S. Clima, R. Degraeve, N. Jossart, O. Richard, T. Vandeweyer, K. Seo, P. Hendrickx, G. Pourtois, H. Bender, L. Altimime, D. J. Wouters, J. A. Kittl, and M. Jurczak, in *IEEE International Electron Devices Meeting (IEDM)*, 2011 (IEEE, Piscataway, NJ, 2011), pp. 31.6.1–31.6.4.
- J. Ramirez, M. Stan, and P. Cristea, *J. Nucl. Mater.* **359**, 174 (2006).
- S. Abolhassani, G. Bart, and A. Jakob, *J. Nucl. Mater.* **399**, 1 (2010).
- B. Mihaila, M. Stan, J. Ramirez, A. Zubelewicz, and P. Cristea, *J. Nucl. Mater.* **394**, 182 (2009).
- H. Matzke, *J. Chem. Soc., Faraday Trans. 2* **83**, 1121 (1987).
- S. Beschmitt and R. A. De Souza, *Solid State Ionics* **305**, 23 (2017).
- T. Zacherle, A. Schriever, R. A. De Souza, and M. Martin, *Phys. Rev. B* **87**, 134104 (2013).
- G. D. Wilk, R. M. Wallace, and J. M. Anthony, *J. Appl. Phys.* **89**, 5243 (2001).
- J. Robertson, *Appl. Surf. Sci.* **190**, 2 (2002).
- J. Robertson, O. Shariya, and A. A. Demkov, *Appl. Phys. Lett.* **91**, 132912 (2007).



- <sup>25</sup>W. Li, J. Zhou, S. Cai, Z. Yu, J. Zhang, N. Fang, T. Li, Y. Wu, T. Chen, X. Xie, H. Ma, K. Yan, N. Dai, X. Wu, H. Zhao, Z. Wang, D. He, L. Pan, Y. Shi, P. Wang, W. Chen, K. Nagashio, X. Duan, and X. Wang, *Nat. Electron.* **2**, 563 (2019).
- <sup>26</sup>A. Hardtdegen, H. Zhang, and S. Hoffmann-Eifert, *ECS Trans.* **75**, 177 (2016).
- <sup>27</sup>M. de Ridder, A. G. J. Vervoort, R. G. van Welzenis, and H. H. Brongersma, *Solid State Ionics* **156**, 255 (2003).
- <sup>28</sup>M. P. Mueller and R. A. De Souza, *Appl. Phys. Lett.* **112**, 051908 (2018).
- <sup>29</sup>L. V. Goncharova, M. Dalponte, D. G. Starodub, T. Gustafsson, E. Garfunkel, P. S. Lysaght, B. Foran, J. Barnett, and G. Bersuker, *Appl. Phys. Lett.* **89**, 044108 (2006).
- <sup>30</sup>S. P. Waldow, H. Wardenga, S. Beschnitt, A. Klein, and R. A. De Souza, *J. Phys. Chem. C* **123**, 6340 (2019).
- <sup>31</sup>Z. Shen, S. J. Skinner, and J. A. Kilner, *Phys. Chem. Chem. Phys.* **21**, 13194 (2019).
- <sup>32</sup>J. Druce, T. Ishihara, and J. A. Kilner, *Solid State Ionics* **262**, 893 (2014).
- <sup>33</sup>J. Druce, H. T  llez, T. Ishihara, and J. A. Kilner, *Faraday Discuss.* **182**, 271 (2015).
- <sup>34</sup>H. Yokokawa, N. Sakai, T. Kawada, and M. Dokiya, in *Science and Technology of Zirconia V*, edited by S. P. S. Badwal and M. J. Bannister (Technomic Publishing Co., Lancaster, Pa., 1993), pp. 59–68.
- <sup>35</sup>R. A. De Souza, J. Zehnpfennig, M. Martin, and J. Maier, *Solid State Ionics* **176**, 1465 (2005).
- <sup>36</sup>R. A. De Souza and M. Martin, *MRS Bull.* **34**, 907 (2009).
- <sup>37</sup>J. P. Perdew, K. Burke, and M. Ernzerhof, *Phys. Rev. Lett.* **78**, 1396 (1997).
- <sup>38</sup>P. E. Bl  chl, *Phys. Rev. B* **50**, 17953 (1994).
- <sup>39</sup>H. J. Monkhorst and J. D. Pack, *Phys. Rev. B* **13**, 5188 (1976).
- <sup>40</sup>G. Henkelman, B. P. Uberuaga, and H. J  nsson, *J. Chem. Phys.* **113**, 9901 (2000).
- <sup>41</sup>G. Henkelman and H. J  nsson, *J. Chem. Phys.* **113**, 9978 (2000).
- <sup>42</sup>H. J  nsson, G. Mills, and K. W. Jacobsen, in *Classical and Quantum Dynamics in Condensed Phased Simulations*, edited by B. J. Berne, D. F. Coker, and G. Cicciotti (World Scientific Publishing Co., 1998), pp. 385–404.
- <sup>43</sup>G. Kresse and J. Furthm  ller, *Phys. Rev. B* **54**, 11169 (1996).
- <sup>44</sup>G. Kresse and D. Joubert, *Phys. Rev. B* **59**, 1758 (1999).
- <sup>45</sup>H. Mehrer, *Diffusion in Solids: Fundamentals, Methods, Materials, Diffusion-Controlled Processes*, Springer Series in Solid-State Sciences Vol. 155 (Springer-Verlag GmbH, Berlin, Heidelberg, 2007).
- <sup>46</sup>I. Kaur, Y. Mishin, and W. Gust, *Fundamentals of Grain and Interphase Boundary Diffusion*, 3rd ed. (Wiley, Chichester, 1995).
- <sup>47</sup>M. Kilo, C. Argirusis, G. Borchardt, and R. A. Jackson, *Phys. Chem. Chem. Phys.* **5**, 2219 (2003).
- <sup>48</sup>R. A. Jackson, A. D. Murray, J. H. Harding, and C. R. A. Catlow, *Philos. Mag. A* **53**, 27 (1986).
- <sup>49</sup>B. Dorado, D. A. Andersson, C. R. Stanek, M. Bertolus, B. P. Uberuaga, G. Martin, M. Freyss, and P. Garcia, *Phys. Rev. B* **86**, 035110 (2012).
- <sup>50</sup>A. Stukowski, *Modell. Simul. Mater. Sci. Eng.* **18**, 025016 (2010).
- <sup>51</sup>J. Wang and U. Becker, *J. Nucl. Mater.* **433**, 424 (2013).
- <sup>52</sup>M. Kilo, R. A. Jackson, and G. Borchardt, *Philos. Mag.* **83**, 3309 (2003).
- <sup>53</sup>V. Metlenko, A. H. H. Ramadan, F. Gunkel, H. Du, H. Schraknepper, S. Hoffmann-Eifert, R. Dittmann, R. Waser, and R. A. De Souza, *Nanoscale* **6**, 12864 (2014).
- <sup>54</sup>N. Bonanos, unpublished work cited by, M. Mogensen, D. Lybye, P. V. Hendriksen, and F. W. Poulsen, *Solid State Ionics* **174**, 279 (2004).
- <sup>55</sup>U. Brossmann, G. Knoner, H.-E. Schaefer, and R. W  rschum, *Rev. Adv. Mater. Sci.* **6**, 7 (2004).
- <sup>56</sup>U. Brossmann, R. W  rschum, U. S  dervall, and H.-E. Schaefer, *J. Appl. Phys.* **85**, 7646 (1999).
- <sup>57</sup>M. Schie, M. P. M  ller, M. Salinga, R. Waser, and R. A. De Souza, *J. Chem. Phys.* **146**, 094508 (2017).
- <sup>58</sup>P.-L. Chen and I.-W. Chen, *J. Am. Ceram. Soc.* **77**, 2289 (1994).
- <sup>59</sup>H. Matzke, *J. Phys. Colloq.* **34**, C9 (1973).
- <sup>60</sup>R. J. Tesch, C. D. Wirkus, and M. F. Berard, *J. Am. Ceram. Soc.* **65**, 511 (1982).
- <sup>61</sup>S. Swaroop, M. Kilo, C. Argirusis, G. Borchardt, and A. H. Chokshi, *Acta Mater.* **53**, 4975 (2005).
- <sup>62</sup>C. Herzig and Y. Mishin, in *Diffusion in Condensed Matter*, edited by P. Heitjans and J. K  rger (Springer-Verlag Berlin Heidelberg, Berlin, Heidelberg, 2005), pp. 337–366.
- <sup>63</sup>D. L. Beke and G. Erdelyi, in *Landolt-B  rnstein: Numerical Data and Functional Relationships in Science and Technology*, Group III Condensed Matter Vol. 33A, edited by O. Madelung and H. Landolt (Springer, Berlin, 1998), pp. 1–26.
- <sup>64</sup>R. W. Balluffi, *Phys. Status Solidi B* **42**, 11 (1970).
- <sup>65</sup>X. Tong, D. S. Mebane, and R. A. De Souza, *J. Am. Ceram. Soc.* **103**, 5 (2020).
- <sup>66</sup>D. van Laethem, J. Deconinck, and A. Hubin, *J. Eur. Ceram. Soc.* **39**, 432 (2019).
- <sup>67</sup>H. J. Avila-Paredes, K. Choi, C.-T. Chen, and S. Kim, *J. Mater. Chem.* **19**, 4837 (2009).
- <sup>68</sup>R. A. De Souza, M. J. Pietrowski, U. Anselmi-Tamburini, S. Kim, Z. A. Munir, and M. Martin, *Phys. Chem. Chem. Phys.* **10**, 2067 (2008).
- <sup>69</sup>X. Guo, W. Sigle, J. Fleig, and J. Maier, *Solid State Ionics* **154–155**, 555 (2002).
- <sup>70</sup>X. Guo and R. Waser, *Prog. Mater. Sci.* **51**, 151 (2006).
- <sup>71</sup>J. P. Parras and R. A. De Souza, *Acta Mater.* **195**, 383 (2020).
- <sup>72</sup>V. A. Gritsenko, D. R. Islamov, T. V. Perevalov, V. S. Aliev, A. P. Yelisseyev, E. E. Lomonova, V. A. Pustovarov, and A. Chin, *J. Phys. Chem. C* **120**, 19980 (2016).
- <sup>73</sup>J. Robertson, *Eur. Phys. J. Appl. Phys.* **28**, 265 (2004).
- <sup>74</sup>X. Zhao and D. Vanderbilt, *Phys. Rev. B* **65**, 233106 (2002).
- <sup>75</sup>Y. Wang, F. Zahid, J. Wang, and H. Guo, *Phys. Rev. B* **85**, 224110 (2012).
- <sup>76</sup>R. A. De Souza, *Phys. Chem. Chem. Phys.* **11**, 9939 (2009).